Earth Planet. Sci. Lett. 624 (2023) 118459

Contents lists available at ScienceDirect

Earth and Planetary Science Letters

journal homepage: www.elsevier.com/locate/epsl

Copper isotope fractionation by diffusion in a basaltic melt

Peng Ni [a,b,*], Anat Shahar [b]

[a] Department of Earth, Planetary and Space Sciences, University of California, Los Angeles, CA 90095, USA
[b] Earth and Planets Laboratory, Carnegie Institution for Science, Washington, DC 20015, USA

ARTICLE INFO

Key words:
Copper isotopes
Diffusive isotope fractionation
Evaporation
Cu-bearing ore deposits
Fluid-rock interaction

ABSTRACT

Copper shows limited isotopic variation in equilibrated mantle-derived silicate rocks, but large isotopic fractionation during kinetic processes. For example, lunar and terrestrial samples that have experienced evaporation were found to have an isotopic fractionation of up to 12.5‰ in their $^{65}Cu/^{63}Cu$ ratios, while komatiites, lherzolites, mid-ocean ridge and ocean island basalts show negligible Cu isotope fractionation as a result of equilibrium partial melting and crystal fractionation. The contrast between the observed magnitudes of equilibrium and kinetic isotope fractionation for Cu calls for a better understanding of kinetic Cu isotope fractionation. One of the mechanisms for creating large kinetic isotopic fractionation even at magmatic temperatures is diffusion. In this study, we performed Cu isotopic measurements on Cu diffusion couple experiments to constrain the beta factor for Cu isotopic fractionation by diffusion. We demonstrate a Monte Carlo approach for the regression and error estimation of the measured isotope profiles, which yielded beta values of 0.16 ± 0.03 and 0.18 ± 0.03 for the two experimental charges measured. Our results are subsequently applied to a quantitative model for the evaporation of a molten sphere to discuss the role of diffusion in affecting the bulk Cu isotopic fractionation between liquid and vapor during evaporation. We apply the model to Cu evaporation experiments and tektite data to show that convection primarily governs mass transport for evaporation during tektite formation. In addition, we show that Cu isotopes can be used as a tool to test the role of kinetics during various magmatic processes such as magmatic sulfide ore deposit formation, porphyry-type ore deposit formation, and fluid-rock interactions.

1. Introduction

Stable isotope geochemistry has been a powerful tool widely applied to almost every branch of geosciences and planetary sciences since its inception. The advancement in multi-collector inductively coupled plasma mass spectrometry (MC-ICP-MS) in the past ~25 years led to the flourish of so-called non-traditional stable isotope geochemistry that enabled routine analysis of a wide range of light and heavy elements (Teng et al., 2017). With improved precision to resolve isotopic variations in natural samples, these newly introduced non-traditional stable isotope systems have become unique tracers of different geological and biological processes based on their distinct geochemical features.

The application of the non-traditional stable isotope systems requires knowledge on how stable isotopes of an element fractionate during physical and chemical processes. Equilibrium isotope exchange reactions and kinetic processes are the two main types of mechanisms that produce mass-dependent stable isotope fractionation in nature. Copper demonstrates relatively small degrees of isotopic fractionation during equilibrium partial melting and crystal fractionation, as indicated by its limited range of isotopic variation among mantle-derived rocks such as mid-ocean basalts, ocean island basalts, komatiites, and peridotites (Savage et al., 2015). For samples that have experienced kinetic processes such as evaporation, however, extremely high degrees of Cu isotope fractionation have been reported. Measurements on lunar soil samples yielded Cu isotopic fractionation of as high as 4.5 ‰ in $\delta^{65}Cu$ (defined as the parts per mil deviation of the $^{65}Cu/^{63}Cu$ ratio relative to the SRM 976 standard; Moynier et al., 2006). In terrestrial impact samples, even higher isotopic fractionation of up to 12.5 ‰ in $\delta^{65}Cu$ have been reported for tektites (Moynier et al., 2010; Rodovská et al., 2017).

The potential of producing large isotopic fractionation at high temperatures makes it especially important to study kinetic processes for the application of non-traditional isotopes to magmatic conditions. Diffusion is a kinetic process that occurs in igneous systems whenever a concentration gradient is generated, such as during mineral growth, mineral dissolution, magma mixing, and evaporation. Mass transport by

* Corresponding author.
E-mail address: pengni@epss.ucla.edu (P. Ni).

https://doi.org/10.1016/j.epsl.2023.118459
Received 1 January 2023; Received in revised form 7 September 2023; Accepted 19 October 2023
Available online 9 November 2023

diffusion is essential for chemical equilibrium to be reached in igneous systems, but significant isotopic fractionation can also be generated during that process, even in a system that is initially isotopically homogeneous (e.g. Richter et al., 1999). In the case of a monatomic ideal gas, the kinetic theory of gasses states that the ratio of diffusivities of two isotopes is equivalent to the inverse square root of their mass ratio (Chapman and Cowling, 1970), with the lighter isotopes diffusing faster than the heavier isotopes. Experimental studies have demonstrated that significant diffusive isotope fractionation could also occur for Ge and Ca in molten oxides (Richter et al., 1999), and for Li, Ca, Mg, Fe, and K in silicate melts (e.g. Richter et al., 2003, 2009; Watkins et al., 2009, 2017; Zhang, 2022). In such condensed systems the mass dependence of diffusive isotope fractionation is complicated by the interactions between the diffusing element and the oxide/silicate matrix and no longer follows the square root law for an ideal gas. Instead, a relationship of $D_1/D_2 = (m_2/m_1)^{\beta}$ inspired by the ideal gas law has been adopted to describe the diffusive isotope fractionation in condensed phases, where D_1, D_2 and m_1, m_2 are the diffusivities and atomic masses of the two isotopes, respectively, and β is an empirical factor between 0 and 0.5 (Richter et al., 1999). The value of β is not an intrinsic property of the condensed phase (e.g. silicate melts), but rather an empirical value that is convenient for describing isotope fractionation by diffusion. Therefore, β values for diffusion in silicate melts need to be determined experimentally and they are critical for quantitatively evaluating diffusive isotope fractionation in igneous processes.

There are numerous reasons why it is interesting to study diffusive isotope fractionation of Cu. As a monovalent cation in silicate melts (except under extremely high oxygen fugacity, e.g. Holzheid and Lodders, 2001), Cu diffusivity is as high as Na in silicate melts (Ni and Zhang, 2016; Ni et al., 2017). Therefore, Cu is expected to have a high value of β factor that can potentially produce large isotope fractionation by diffusion during non-equilibrium processes. Copper has a half condensation temperature of 1037 K and behaves as a moderately volatile element (Lodders, 2003). Copper isotopes are therefore suitable for tracing evaporation processes such as tektite-forming meteorite impacts (Moynier et al., 2010; Rodovská et al., 2017), the trinitite-forming nuclear detonation (Day et al., 2020), and evaporation processes that occurred during the Moon-forming giant impact or operated on the lunar surface after Moon formation (e.g. Moynier et al., 2006; Day et al., 2019; Nie and Dauphas, 2019). Further, diffusive isotope fractionation could contribute significantly to the heavy isotope enrichment of Cu in the evaporated residue during evaporation processes (e.g. Sossi et al., 2020).

In addition to its moderate volatility in nature, Cu also behaves as a siderophile and highly chalcophile element (e.g. Siebert et al., 2011), making it sensitive to sulfide-bearing partial melting, magma crystallization, and core formation processes. When complexed with Cl or S, Cu could preferentially partition into magmatic volatile phases, providing a mechanism for the efficient enrichment and transport of Cu through a fluid-saturated magma chamber in the upper continental crust, which ultimately leads to the formation of Cu-bearing porphyry-type ore deposits (e.g. Candela, 1997; Zajacz et al., 2011; Huber et al., 2012). These igneous processes involving sulfides, metals, and magmatic volatile phases are often assumed to be equilibrium processes for simplification. This assumption, however, has been challenged when more sophisticated models are used to describe core formation or porphyry-type ore formation processes (e.g. Huber et al., 2012; Marchi et al., 2018). The potential role of kinetic control in magmatic processes makes it important to understand how Cu isotopes fractionate kinetically by diffusion.

More generally, as a moderately volatile, siderophile, and strongly chalcophile element, the geochemical behavior of Cu is sensitive to a wide range of magmatic processes. Diffusive Cu isotope fractionation could play a significant role in fractionating Cu isotopes at magmatic temperatures. As discussed above, a quantitative understanding of the magnitude of Cu isotope fractionation by diffusion requires knowledge of its β factor, which has not been constrained. In this paper, we report experimentally constrained β factors for Cu isotope fractionation by diffusion in basaltic melts. We show that Cu diffusion in silicate melts is capable of producing very large isotopic fractionation in Cu. Our experimentally constrained β factor is essential for quantitatively incorporating diffusive Cu isotope fractionation in current and future studies of kinetic magmatic processes, such as evaporation, Cu-bearing ore deposit formation, and water-rock interactions.

2. Experimental and analytical methods

Two experimental charges of Cu diffusion couple experiments from the study of Ni and Zhang (2016) were selected for this study. Details of the experiment design can be found in Ni and Zhang (2016) and are briefly summarized below. Two basaltic glasses with the same target major element composition but different copper concentrations were synthesized using a gas-mixing furnace. A mixture of oxides and carbonates was used as the starting material for both glasses. A 99.9% pure Cu_2O powder from Alfa Aesar was used as the source of Cu in the Cu-rich basaltic glass Et1Cu (with ~1000 ppm Cu), while all Cu in the Cu-poor basaltic glass Et1 (with ~100 ppm Cu) came from impurities in the commercial oxides and carbonates. The compositions of the two starting glasses are reported in Table S1. The synthesized glasses were prepared into cylinders and a wafer of each cylinder was cut and used for the diffusion couple experiments. The diffusion couple experiments were conducted using a piston-cylinder apparatus with graphite capsules and a barium carbonate pressure medium. The two experimental charges selected for this study are from a complete series of 10 experiments conducted at temperatures of 1298 to 1581 °C with durations of 2 to 7 min. The two experiments, Cudiffcp 1.2 and Cudiffcp 2.1, were both conducted at 1 GPa, and at temperatures of 1314 °C for 162 s and 1397 °C for 163 s, respectively. Choice of experiments for this study was mainly limited by the spatial resolution of the micro-drill sampling technique, which requires both the diffusion profile and the far field to be 300 μm or longer.

Each diffusion couple experiment charge was sampled for Cu isotope analysis using a Newwave micromill equipped with 300-μm-diameter tungsten carbide drill bits. For each drilling attempt, the surface of the sample charge was cleaned with Milli-Q water and compressed air. Subsequently, a drop of Milli-Q water was placed at the drilling position to collect the drilled materials. Each drilling attempt penetrated 400 to 500 μm into the sample and the drilled materials were transferred into a Teflon vial by pipetting Milli-Q water at the drilling site repeatedly. In order to collect sufficient materials for Cu isotope analysis, drilling was repeated up to 5 times at the same distance to the diffusion interface and the drilled materials were combined. This was especially the case for the end with low Cu concentrations. To avoid cross contamination, drilling was conducted from the low concentration end to the high concentration end. At each distance to the interface, the surface of the sample charge was cleaned with Milli-Q water and compressed air to remove any residue of drilled particles. In total, eight samples were collected along the diffusion profile for each of the two experiments. Based on the drilled volume, approximately 100 to 480 μg of basaltic glasses were collected for each sample, yielding ~30 to 260 ng of Cu after column chemistry. In addition to the two experimental charges, a cross-section of the starting glass Et1Cu was also sampled using the same approach, but using a drill bit diameter of 500 μm and a drilling depth of 200 μm. After drilling, milli-Q water in the beakers was evaporated on a hot plate and a 2:1 mixture of concentrated HF:HNO_3 was used for sample digestion.

The chemical purification procedure for Cu in this study utilizes a long column procedure modified from previous studies (e.g. Maréchal et al., 1999; Sossi et al., 2015) and is essentially identical to previously reported in Ni et al. (2021). The only exception is that BioRad quartz columns instead of homemade quartz columns were used for Cu separation in this study. The calibrated elution curve is reported in Fig. S1 and the procedure is briefly described below. More details about the Cu isotope analysis can be found in Ni et al. (2021). Sample aliquots were

dried down and taken up again multiple times using concentrated HCl, before being loaded onto 0.5-cm-diameter BioRad quartz glass columns filled with 5.5 cm BioRad AG1-X8 (200–400 mesh) resin for Cu separation. Matrix elements were eluted in 8 ml of 8 M HCl and the Cu fraction was then eluted in another 9.5 ml of 8 M HCl. The eluted Cu sample was evaporated to dryness and the purification procedure was repeated once to further purify Cu. The final products were taken up in 0.4 M nitric acid for analysis. Copper isotope analysis was performed under the wet plasma mode on a Nu Plasma II Multi-Collector Inductively-Coupled-Plasma Source Mass-Spectrometer at the Carnegie Institution for Science. The sample aliquots were diluted to 10 or 20 ppb in concentration for analysis. The sensitivity was ~30 to 40 V/ppm for ^{63}Cu, which was sufficient to achieve analytical errors of ~0.3 ‰ (2 standard deviation) even for 10 ppb Cu solutions (Ni et al., 2021). Corrections for instrumental mass bias were achieved by standard-sample bracketing using the ERM-AE633 standard, which is a reference material from the Joint Research Center that has an isotopic composition 0.01‰ lighter than the discontinued international Cu standard NIST SRM 976. Each sample was measured 6 to 8 times with each measurement consisted of 20 cycles with 4 s of integration. Variations in Cu ratios in this study are reported using the delta notation as follows: $\delta^{65}Cu = [(^{65}Cu/^{63}Cu_{sample})/(^{65}Cu/^{63}Cu_{SRM976}) - 1] \times 1000‰ = [(^{65}Cu/^{63}Cu_{sample})/(^{65}Cu/^{63}Cu_{AE633}) - 1] \times 1000 + 0.01‰$ (Moeller et al., 2012). Copper isotope measurements of geological standards, BHVO-2 and AGV-2, yielded δ^{65}Cu values of 0.15 ± 0.01‰ (2 s.e.) and 0.10 ± 0.03‰ (2 s.e.), respectively, which are consistent with recommended values of 0.12 ± 0.02‰ and 0.04 ± 0.04‰ in Moynier et al. (2017).

3. Results

For each of the two diffusion couple experiments, eight Cu isotopic measurements were conducted at distances ~400 μm apart from each other along the diffusion profile. As an example, locations of the electron microprobe analyses for Cu concentrations (Ni and Zhang, 2016) and the drill holes for Cu isotopic measurements are shown in Fig. 1 for experiment Cudiffcp 1.2. Distance measurement for the isotopic composition profiles was performed by assuming the same interface location as in Ni and Zhang (2016) for the Cu concentration profiles.

The measured Cu isotopic composition profiles for both experiments are plotted in the lower panels of Fig. 2. From the high concentration end to the low concentration end, the δ^{65}Cu value varies significantly from as high as +4.8‰ to as low as −7.5‰, with a total variation of over 10‰. The large total variation in δ^{65}Cu is mostly due to the difference in the initial Cu isotope composition between the two basaltic glasses, which was heavy for the high-Cu glass (Et1Cu) but light for the low-Cu glass (Et1). The measured Cu isotopic composition of ~4.2‰ on the high concentration end of the two diffusion couple charges is consistent with independent measurements of the high-Cu initial glass Et1Cu, as will be discussed in more detail later. On the other hand, the low-Cu glass Et1 was exhausted for use in the diffusion couple experiments and no sufficient initial glass is available for similar measurements. Despite the large difference in initial δ^{65}Cu composition of the two starting glasses, both experiments show a slight increase in δ^{65}Cu on the high-concentration end and decrease on the low-concentration end of the diffusion front (Fig. 2), which is characteristic for isotopic fractionation by diffusion (e.g. Richter et al., 2003).

3.1. Modeling the $^{65}Cu/^{63}Cu$ fractionation profiles

Regression of the Cu concentration profiles was performed in Ni and Zhang (2016) using the solution to the one-dimensional diffusion couple problem (Crank, 1975):

$$C = \frac{C_0 + C_1}{2} + \frac{C_0 - C_1}{2}\,\mathrm{erf}\frac{x - x_0}{\sqrt{4Dt}}, \quad (1)$$

where C_0 and C_1 are the initial Cu concentration on the low-Cu and high-Cu far-field of the diffusion couple, respectively; D is the Cu diffusivity; and x_0 is the position of the diffusion couple interface. Fitting the concentration profiles of the two experiments yielded diffusivities of 439 ± 27 μm^2/s at 1314 °C (Cudiffcp 1.2) and 678 ± 44 μm^2/s at 1397 °C (Cudiffcp 2.1) in Ni and Zhang (2016), which are reproduced in the upper panels of Fig. 2. A Cu concentration of 0.132 wt% best fit the high-Cu end of the diffusion couples, while that for the low-Cu end was found to be 0.016 and 0.018 wt% based on the regression (Fig. 2).

Regression of the Cu isotope fractionation profile was conducted assuming that the diffusivity of ^{63}Cu and ^{65}Cu is proportional to the inverse of their mass ratio:

$$\frac{D_{65}}{D_{63}} = \left(\frac{m_{63}}{m_{65}}\right)^{\beta}, \quad (2)$$

where D_{63}, D_{65}, m_{63}, and m_{65} are the diffusivities and masses of ^{63}Cu and ^{65}Cu, respectively, while β is the empirical factor to be constrained by regression. The ratio of ^{65}Cu/^{63}Cu ($R_{65/63}$) along the diffusion couple can be calculated using the following relationship:

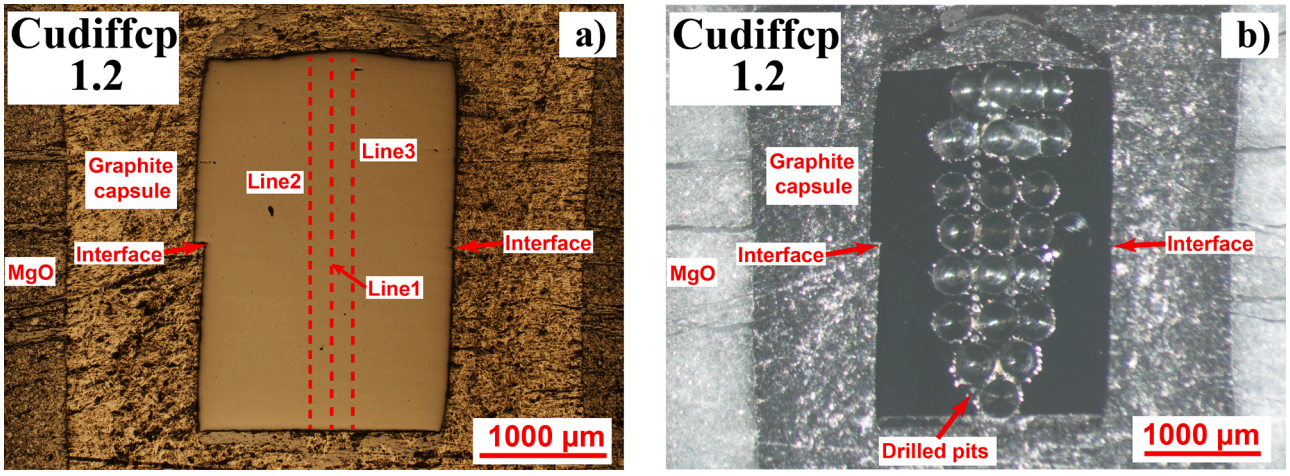

Fig. 1. a) Petralogical microscope image of experimental charge Cudiffcp 1.2 showing different parts of the assembly and locations of three electron microprobe traverses analyzed in Ni and Zhang (2016). b) Binocular microscope image of the same experimental charge after being sampled using a micromill for Cu isotopic measurements.

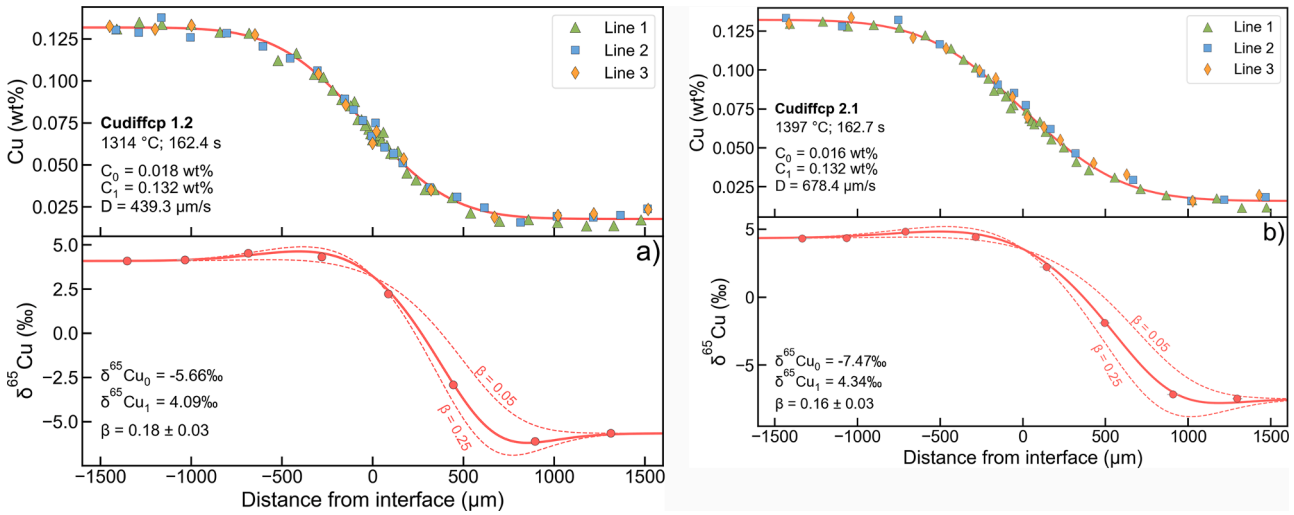

Fig. 2. Copper concentration and isotopic composition profiles of the two diffusion couple experiments a) Cudiffcp 1.2 and b) Cudiffcp 2.1. Different traverses of the electron microprobe analyses are plotted using different symbols in the upper panel for each experiment. Best fit of the concentration and isotopic composition profiles are plotted in red solid curves. The fitting results of each profile are shown at the lower left corner of the panel. Electron microprobe data for Cu concentration profiles and the fitting results are from Ni and Zhang (2016). More details about the regression are discussed in the main text.

$$R_{65/63} = \frac{\frac{1}{2}\left(C_{0,65} + C_{1,65}\right) + \frac{1}{2}\left(C_{0,65} - C_{1,65}\right)\mathrm{erf}\frac{x-x_0}{\sqrt{4D_{65}t}}}{\frac{1}{2}\left(C_{0,63} + C_{1,63}\right) + \frac{1}{2}\left(C_{0,63} - C_{1,63}\right)\mathrm{erf}\frac{x-x_0}{\sqrt{4D_{63}t}}}, \quad (3)$$

where $C_{0,63}$, $C_{0,65}$, $C_{1,63}$, and $C_{1,65}$ are the initial concentrations of ^{63}Cu and ^{65}Cu on the low and high concentration ends, respectively. With initial δ^{65}Cu values of δ_0 and δ_1 (in per mil) for the low and high concentration ends, eq. (3) can be expressed in delta notation as:

$$\delta^{65}\mathrm{Cu} \approx \left\{ \frac{\left[\left(\frac{\delta_0}{1000}+1\right) + B\left(\frac{\delta_1}{1000}+1\right)\right] + \left[\left(\frac{\delta_0}{1000}+1\right) - B\left(\frac{\delta_1}{1000}+1\right)\right]\mathrm{erf}\frac{(x-x_0)}{\sqrt{4(m_{65}/m_{63})^{\beta}D_{63}t}}}{(1+B)+(1-B)\mathrm{erf}\left[\frac{(x-x_0)}{\sqrt{4D_{63}t}}\right]} - 1 \right\} \times 1000‰, \quad (4)$$

where $B = C_1/C_0$ is the initial concentration ratio of the two ends of the diffusion couple. Because only 8 isotopic measurements were conducted for each diffusion couple experiment, it is not feasible to fit all the 6 parameters (δ_0, δ_1, B, x_0, D_{63}, and β) simultaneously. Instead, regression of the isotopic fractionation profile focused on constraining the β factor only, while values for the other 5 parameters were obtained independently. Among these five parameters, x_0 and D_{63} (assumed to be equal to D) were constrained by fitting the electron microprobe data (Ni and Zhang, 2016; reproduced in Fig. 2 top panel). Copper isotope compositions of the initial glasses (δ_0, δ_1) were set to be equal to the measured data points at the far fields of the diffusion couple. Based on the regression of the diffusion profiles, these data points were unaffected by diffusion. Similarly, the values of C_0 and C_1 were set to be 125 ppm and 1190 ppm for Cudiffcp 1.2, and 103 ppm and 1164 ppm for Cudiffcp 2.1 based on wet chemistry measurements of the far-field Cu concentrations (Table S2), which indicates a B value of 9.5 and 11.3 for these two experiments, respectively. Note that although the electron microprobe analysis provided Cu concentration data with higher spatial resolution at the far-fields of the experiments, it is less accurate in determining the absolute concentrations at the 100 ppm level (Ni and Zhang, 2016).

Assuming $\delta_0 = -5.66‰$, $\delta_1 = 4.09‰$, $x_0 = 10$ μm, $D_{63} = 439.3$ μm^2/s, and $B = 9.5$ for experiment Cudiffcp 1.2, a beta value of 0.18 can be obtained based on the Cu isotope fractionation profile along the diffusion couple. Similarly, assuming $\delta_0 = -7.47‰$, $\delta_1 = 4.34‰$, $x_0 = 8$ μm, $D_{63} = 678.4$ μm^2/s, and $B = 11.3$, the beta value for Cudiffcp 2.1 can be constrained to be 0.16. In order to make sure that the beta factors are reliable, the predicted δ^{65}Cu profiles with $\beta = 0.05$ and 0.25 are modeled using eq. (4) and plotted in Fig. 2 for comparison. It is apparent based on the comparison that the measured Cu isotope fractionation profiles would differ significantly from the prediction if the beta factor is as low as 0.05 or as high as 0.25. Another way to better demonstrate the effect of diffusion on Cu isotope fractionation is to correct the measured Cu isotope profile by the purely mixing profile ($\beta = 0$):

$$\delta^{65}\mathrm{Cu}_{\mathrm{cr}} = \delta^{65}\mathrm{Cu} - \delta^{65}\mathrm{Cu}_{\mathrm{mix}} = \delta^{65}\mathrm{Cu} - \left\{ \frac{\left[\left(\frac{\delta_0}{1000}+1\right) + B\left(\frac{\delta_1}{1000}+1\right)\right] + \left[\left(\frac{\delta_0}{1000}+1\right) - B\left(\frac{\delta_1}{1000}+1\right)\right]\mathrm{erf}\left[\frac{(x-x_0)}{\sqrt{4D_{63}t}}\right]}{(1+B)+(1-B)\mathrm{erf}\left[\frac{(x-x_0)}{\sqrt{4D_{63}t}}\right]} - 1 \right\} \times 1000‰ \quad (5)$$

The above equation is especially useful for highlighting the isotopic fractionation caused by diffusion when the initial isotopic compositions on the two ends of the diffusion couple differ significantly. If diffusion did not cause any isotopic fractionation, $\delta^{65}Cu_{cr}$ is expected to be 0‰ across the entire diffusion couple and beta should be zero. Any beta values significantly higher than zero should lead to positive $\delta^{65}Cu_{cr}$ values on the high-concentration end of the diffusion couple and negative $\delta^{65}Cu_{cr}$ values at the diffusion front toward the low-concentration end, which is exactly the case for the two experiments conducted in this study (Fig. S3). Note that fitting the $\delta^{65}Cu$ and the $\delta^{65}Cu_{cr}$ profiles is expected to yield the same beta values because regression using eq. (4) or (5) is mathematically identical.

3.2. Error estimation

The measured Cu isotope profiles were fit very well by eq. (4) and eq. (5), as can be seen in Fig. 2 or Fig. S3. Error estimation based on the misfit of the data yielded negligible errors for the beta factors. To obtain a more realistic estimation of the error for the beta factor, uncertainties projected from major parameters in eq. (4) including δ_0, δ_1, D_{63}, and B are considered. Contributions from the uncertainties of x_0 (<10 μm) are negligible and hence excluded in error estimation. Uncertainties in the initial Cu concentration and Cu isotope composition of the starting glass are investigated by analyzing a center section of the high-Cu glass Et1Cu (Fig. S4a). Electron microprobe analysis shows that the Cu concentration of the glass varies by approximately 30% from 0.13 wt% to 0.10 wt % across the entire 7 mm profile of the glass. The Cu isotopic composition, on the other hand, varies from 3.6 to 5.0‰ across the same cross section. Considering the fact that 1.5 mm wafers of the initial glass were used for experiments and the edge of the glass was avoided, the uncertainties on Cu concentration (C_1) and Cu isotopic composition (δ_1) can be estimated to be approximately 15% and 0.5‰, respectively. Unfortunately, no sufficient glass for Et1 was left for a similar investigation on the low-Cu glass for C_0 and δ_0. The uncertainties are therefore assumed to be the same as those for C_1 and δ_1 because the two glasses were synthesized using identical procedures. The uncertainties on D_{63} are based on fitting of the diffusion profiles and are 12% relative (2σ) for Cudiffcp 1.2 and Cudiffcp 2.1 (Ni and Zhang, 2016). Note that here D_{63} is assumed to be equal to D, but more strictly D is equal to the abundance weighted average of the diffusivities of ^{65}Cu and ^{63}Cu. However, the difference between D and D_{63} is within 0.5% and the effect of this approximation on the final results is negligible.

With the estimated uncertainties on the key parameters, a Monte Carlo approach was employed to investigate the uncertainties on the beta factors constrained by our experiments. Random numbers are generated for δ_0, δ_1, B and D_{63} assuming that their uncertainties follow the Gaussian distribution. According to the above estimation of error for these parameters, it is assumed that δ_0 and δ_1 have one sigma absolute error of 0.25‰, while B and D_{63} have one sigma variance of 10.5% and 6%, respectively. The randomly generated values for these four parameters were subsequently used for regression with eq. (4) to fit the measured Cu isotopic profiles. About one million Monte Carlo runs were conducted for each experiment and the set of beta values yielded by the simulations show approximate Gaussian distribution (Fig. S5). The mean and variance of the set of beta factors obtained via this approach are 0.18 ± 0.03 (2σ) for Cudiffcp 1.2 and 0.16 ± 0.03 (2σ) for Cudiffcp 2.1, respectively.

4. Discussion

4.1. Comparison to literature studies

The beta factors of 0.18 ± 0.03 and 0.16 ± 0.03 determined for Cu diffusion in this study can be compared with literature data on other elements in the silicate melt system. To the best of our knowledge, experimentally determined beta factors for isotopic fractionation in silicate melts cover a list of six elements (Li, Ca, Mg, Fe, K, and Cu) and span a wide range from 0.030 to 0.228. Among these elements, Cu has relatively large beta factors that are only smaller than Li in basaltic/rhyolitic melts and Ca in albite/anorthosite/diopside melts (Richter et al., 2003; Watkins et al., 2011; Holycross et al., 2018). It has been previously proposed (e.g. Watkins et al., 2017; Holycross et al., 2018) that the beta factor for isotopic fractionation of an element (i) in silicate melts may be correlated with its Si-normalized effective binary diffusivity (D_i/D_{Si}). The mechanism used to explain this concept was that faster diffusing elements are more likely moving in the silicate melt network as single atoms or oxide complexes, therefore interacting less with other network elements and show greater isotope mass

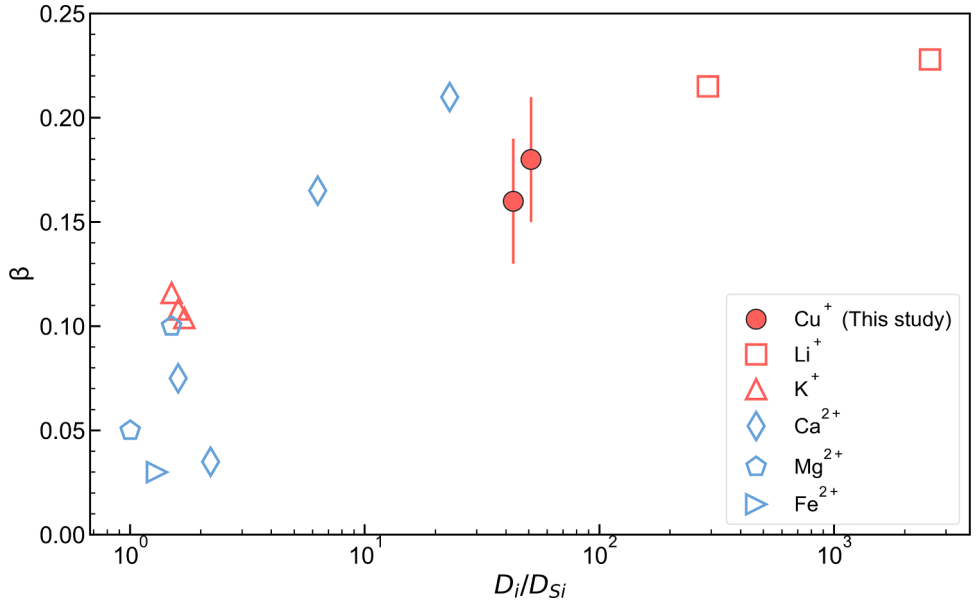

Fig. 3. Experimentally determined β factors of an element i plotted versus its Si-normalized diffusivity in silicate melts. The errors plotted for Cu are estimated based on uncertainties propagated from the inhomogeneities of the starting samples and the diffusivity. Literature values are plotted in open symbols (Holycross et al., 2018; Richter et al., 2003, 2008; F.M. 2009; Watkins et al., 2009, Watkins et al., 2011; Zhang, 2022). The monovalent and bivalent cations are plotted in different colors for distinction.

discrimination. The recently added beta factor data for potassium were generally consistent with this trend (Zhang, 2022), but our data for Cu are on the low side of the existing trend in literature (Fig. 3). Copper diffusion in basalt is only slightly lower than lithium and as fast as sodium. Using silicon self-diffusion data summarized in Zhang et al. (2010), D_{Cu}/D_{Si} ratios for our two experiments can be calculated to be 51 and 43, between the Si-normalized diffusivities for Li in basaltic/rhyolitic melts and for Ca in albite/anorthosite/diopside melts. The beta factors for Cu (0.18 ± 0.03 and 0.16 ± 0.03), however, are lower than those determined for Li (0.215 and 0.228) and Ca (0.165 and 0.210), as shown in Fig. 3. One possible explanation is that the trend expected between beta factor and Si-normalized diffusivity depends on valence state. Among the elements studied so far, Li, Cu, and K are monovalent, while Ca, Mg, and Fe are divalent. These two groups of elements define different trends in Fig. 3. The beta factor of K^+ is higher than divalent cations with the same D_i/D_{Si}, whereas that of Cu^+ falls to the lower end of divalent cations. More generally, the departure of Cu beta factors from the previously defined trend indicates that such a correlation is rather qualitative than quantitative. As previously pointed out by Zhang (2022), about half of the variation in β is within a narrow range of D_i/D_{Si} ratios, making it difficult to quantitatively define the correlation between β and Si-normalized diffusivity.

4.2. Modeling Cu isotope fractionation during evaporation in a diffusion-limited regime

As a moderately volatile element, Cu is sensitive to evaporation processes such as magma ocean evaporation, tektite-forming meteorite impacts, the Moon-forming giant impact, and nuclear detonation (e.g. Moynier et al., 2010; Norris and Wood, 2017; Rodovská et al., 2017; Nie and Dauphas, 2019; Day et al., 2019, 2020). A scenario commonly involved in laboratory experiments (e.g. Ni et al., 2021; Sossi et al., 2019, 2020; Zhang et al., 2021) and modeling of magma ocean evaporation (e.g. Young et al., 2019) is the evaporative loss of moderately volatile elements from a molten silicate sphere (Fig. 4a). Here we adapt this scenario as an example to discuss how diffusion affects Cu isotope fractionation during evaporation.

In an evaporating molten sphere, if mass transport within the sphere is purely by diffusion, the differential equation that describes the concentration profile of an evaporate can be written as:

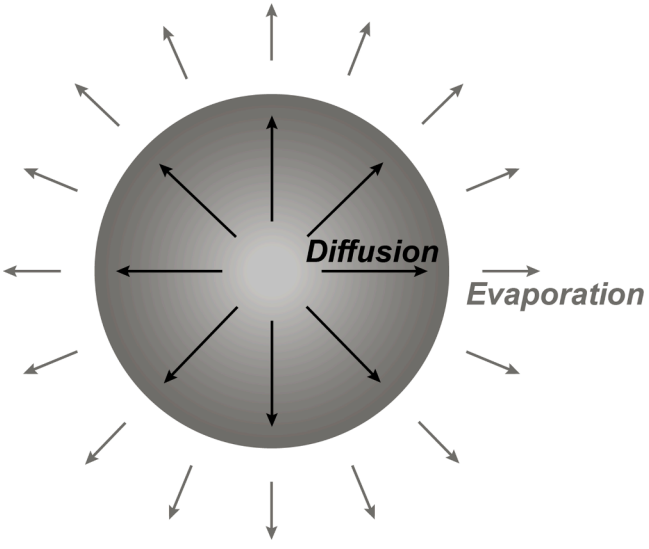

Fig. 4. Schematic view of diffusion-controlled surface evaporation of a molten sphere. Components in the liquid are transported to the liquid-vapor interface by diffusion and subsequently lost to the vapor phase by evaporation.

$$\frac{\partial C}{\partial t} = D\frac{\partial^2 C}{\partial r^2} + \frac{2D}{r}\frac{\partial C}{\partial r}, \tag{6}$$

where C and D are the concentration and diffusivity of the element of interest, whereas r and t stand for radius and time, respectively. The above boundary conditions assume a constant radius for the evaporating sphere, which is applicable to the evaporation of trace elements (including Cu) in the liquid. Evaporation of major elements involves the shrinkage of the sphere and needs to be solved differently using a numerical approach (Young et al., 1998). Assuming the initial concentration to be uniform and considering the fact that the diffusive flux equals the evaporative flux at the liquid-vapor interface, the initial and boundary conditions can be defined as:

$$C|_{t=0} = C_0,\ 0 \le r \le R_0, \tag{7}$$

$$-D\frac{\partial C}{\partial r}|_{r=0} = 0, \tag{8}$$

$$-D\frac{\partial C}{\partial r}|_{r=R} = J_{Evap} = \nu C. \tag{9}$$

In the above equations, C_0 is the initial concentration of the desired element in the melt sphere, R_0 is the radius of the melt sphere, J_{Evap} is the evaporation flux, and ν is the evaporation coefficient. It has been shown in Zhang et al. (2021) that the isotopic fractionation factor between vapor and residue ($\alpha^{i/j}_{vapor-residue}$) can be expressed in an approximate solution to eqs. (6-9):

$$\alpha^{i/j}_{vapor-residue} = [1 - w(L)]\frac{D_j}{D_i} + w(L)\frac{\upsilon_j}{\upsilon_i}, \tag{10}$$

where D_j/D_i and υ_j/υ_i are the diffusivity and evaporation coefficient ratios of two isotopes j and i of the desired element. The weight function in eq. (10) is defined as:

$$w(L) = \frac{2L}{L - 1 + (L-1)^2/\cos^2(\theta_1)}, \tag{11}$$

where $L = \upsilon R_0/D$ is a dimensionless parameter proportional to the ratio of the diffusion time scale ($\tau_{Diff} = {R_0}^2/D$) and the evaporation time scale ($\tau_{Evap} = R_0/3\upsilon$), whereas θ_1 is the first positive root of the transcendental equation:

$$\theta\cot\theta - 1 + L = 0. \tag{12}$$

From eq. (10), consider that $D_j/D_i = (m_i/m_j)^\beta$ and $\upsilon_j/\upsilon_i = (m_i/m_j)^\zeta$ with β being the isotopic fractionation exponent for diffusion (eq. (2)) and ζ the isotopic fractionation exponent for evaporation at the vapor/melt interface, we obtain (Zhang et al., 2021):

$$\alpha^{i/j}_{vapor-residue} = [1 - w(L)]\left(\frac{m_i}{m_j}\right)^\beta + w(L)\left(\frac{m_i}{m_j}\right)^\zeta. \tag{13}$$

In the case of Cu, our experiments show that β has a value of 0.17 for Cu diffusion in silicate melts. The value of ζ, on the other hand, is related to the vapor saturation index (defined as $s = P/P_{sat}$, partial pressure divided by the equilibrium partial pressure of the desired element) via the following equation (Dauphas et al., 2015; Nie and Dauphas, 2019):

$$1000\left(\left(\frac{M_i}{M_j}\right)^\zeta - 1\right) = \Delta_{Evaporation} = \Delta_{Equilibrium} + (1-s)\Delta_{Kinetic}. \tag{14}$$

For free evaporation ($s = 0$) at high temperatures above silicate liquidus, $\Delta_{Equilibrium}$ is usually small enough to be safely ignored, while $\Delta_{Kinetic}$ for evaporation into vacuum can be reasonably assumed to be (Nie and Dauphas, 2019):

$$\Delta_{Kinetic} = 1000\left(\sqrt{\frac{m_i}{m_j}} - 1\right). \tag{15}$$

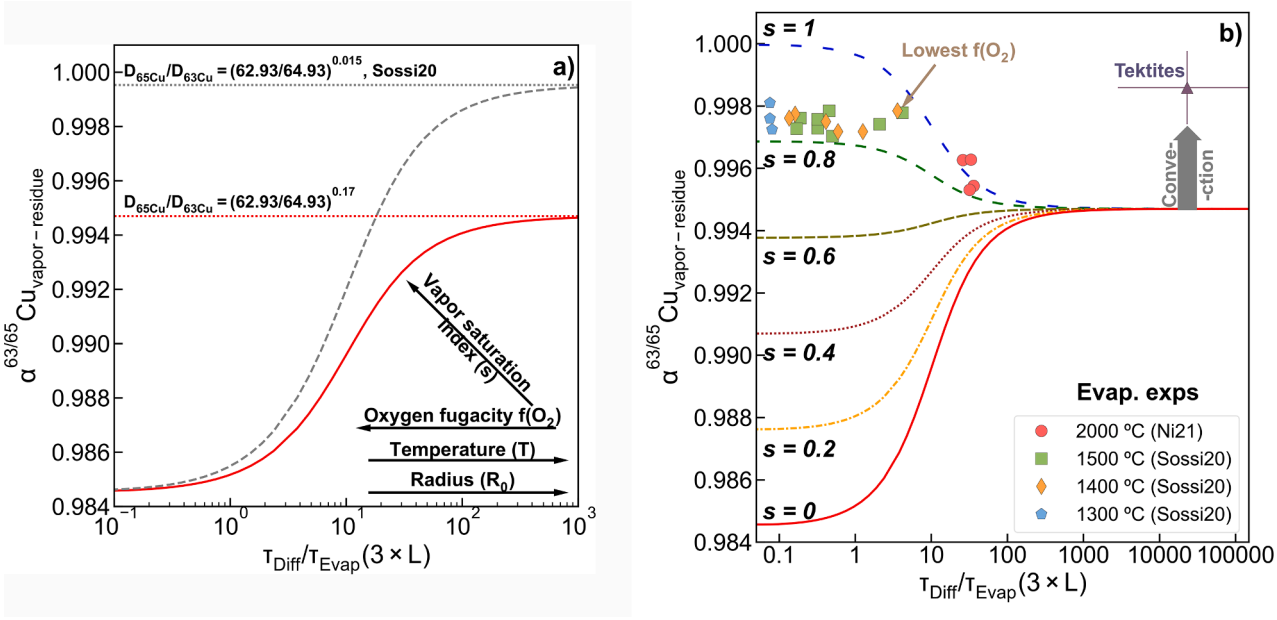

Fig. 5. a) Calculated Cu isotope fractionation factors between vapor and bulk residues as a function of the diffusion time scale (τ_{Diff}) divided by the evaporation time scale (τ_{Evap}). The red solid curve is calculated using $\beta = 0.17$ as determined in this study, while the gray dashed curve is calculated assuming $\beta = 0.015$ following Sossi et al. (2020). At low τ_{Diff}/τ_{Evap} ratios, the fractionation factor is controlled by evaporation, while at high τ_{Diff}/τ_{Evap} ratios it is controlled by diffusion. b) Calculated curves for different vapor saturation conditions (s). Higher vapor saturation suppresses isotopic fractionation at the vapor/liquid interface and reduces the bulk isotope fractionation factor for the diffusion-unlimited regime ($\tau_{Diff}/\tau_{Evap}<0.1$). The calculated values for evaporation experiments (Ni et al., 2021; Sossi et al., 2020) and tektites (Moynier et al., 2010; Rodovská et al., 2017) are also plotted. The error bars for tektites reflect the uncertainties in radius, Cu evaporation rate, and the range of empirical α values in literature (see supplementary text for detail).

Combining eq. (15) and eq. (14) and assume $\Delta_{Equilibrium} = 0$, we obtain $\zeta = 0.5$ for free evaporation of Cu. With $\beta = 0.17$ and $\zeta = 0.5$, and by numerically solving eq. (12) to obtain θ_1, Cu isotope fractionation factor for an evaporating melt sphere in the diffusion-limited regime can be calculated using the following equation:

$$\alpha^{63/65}Cu_{vapor-residue} = [1 - w(L)]\left(\frac{m_{63}}{m_{65}}\right)^{0.17} + w(L)\left(\frac{m_{63}}{m_{65}}\right)^{0.5}. \quad (16)$$

The calculated $\alpha^{63/65}Cu_{vapor-residue}$ values as a function of τ_{Diff}/τ_{Evap} are plotted in Fig. 5a. As shown in the figure, in the diffusion-unlimited regime where $\tau_{Diff}/\tau_{Evap} < 0.1$, the bulk isotopic fractionation factor is controlled by free evaporation at the melt/vapor interface ($\alpha^{63/65}Cu = (63/65)^{0.5}$). In the highly diffusion-limited regime where $\tau_{Diff}/\tau_{Evap} > 1000$, the bulk isotopic fractionation factor is dominated by the diffusivity difference of the Cu isotopes ($\alpha^{63/65}Cu = (63/65)^{0.17}$). The calculated curve differs from what was calculated in Sossi et al. (2020) based on a lower value of 0.015 (gray curve in Fig. 5a). A high β value of 0.17 for Cu diffusion determined in this study indicates that in the case of diffusion-limited evaporation, the bulk isotopic fractionation between vapor and melt is large no matter if the process is diffusion-controlled or surface evaporation controlled.

4.3. Application to evaporation experiments and tektite formation

Next, we explore how the above model applies to Cu evaporation experiments and tektite data in literature. In order to do so, it is crucial to calculate the value of τ_{Diff}/τ_{Evap}, which equals $3\nu R_0/D$. Experimentally determined Cu diffusivities (D_{Cu}) in basaltic (Ni and Zhang, 2016) and rhyolitic melts (Ni et al., 2018, 2017) are available in literature, leaving evaporation coefficient (ν) as the key parameter to constrain for calculating τ_{Diff}/τ_{Evap} in the above model.

One way to constrain the value of ν comes from its connection to the Hertz-Knudsen equation, which describes the evaporative flux for a particular species through the surface of a melt sphere:

$$-J_{HK} = \frac{dn}{dt} = -4\pi R_0^2 \frac{\alpha_{ec}(P_{sat} - P)}{\sqrt{2\pi RMT}}, \quad (17)$$

where J_{HK} or dn/dt is the evaporative flux in mol/s, P_{sat} is the equilibrium partial pressure, P is the partial pressure at the surface, R_0 is the radius of the sphere, M is the molar mass, R is the gas constant, T is the temperature in K, and α_{ec} is the dimensionless evaporation/condensation coefficient ($0 < \alpha_{ec} < 1$). For diffusion-unlimited evaporation from a melt sphere whose composition and radius does not change significantly, it has been previously shown in Sossi et al. (2019) and Ni et al. (2021) that eq. (17) can be solved to give:

$$\frac{dC}{dt} = -\frac{3\alpha_{ec}(1-s)\gamma K}{R_0 \rho f(O_2)^{n/4}} \frac{M_{melt}}{\sqrt{M}} \sqrt{\frac{1}{2\pi RT}} C, \quad (18)$$

where s is the saturation index defined as $s = P/P_{sat}$, M_{melt} is the average molar mass of the melt, ρ is the density of the melt, $f(O_2)$ is the oxygen fugacity, while K and n are the equilibrium constant and number of electron transfer for the evaporation reaction of metal M:

$$MO_{(x+n)/2}(l) = MO_{x/2}(g) + \frac{n}{4}O_2. \quad (19)$$

In the case of Cu, $x = 0$ and $n = 1$ for eq. (19) because it dissolves in silicate melt as $CuO_{0.5}$ and evaporates in the form of Cu metal (Ni and Zhang, 2016; Sossi et al., 2019). Using eq. (18) and based on mass balance, we obtain:

$$J_{Evap} = \nu C = -\frac{dC}{dt} \times \frac{V}{S_{area}} = -\frac{dC}{dt} \times \frac{R_0}{3}. \quad (20)$$

Hence:

$$\nu = \frac{\alpha_{ec}(1-s)\gamma K}{\rho f(O_2)^{n/4}} \frac{M_{melt}}{\sqrt{M}} \sqrt{\frac{1}{2\pi RT}}. \quad (21)$$

Experimental studies on the evaporation of moderately volatile elements rarely aim at obtaining ν from the data. Alternatively, the solution

to the Hertz-Knudsen equation (eq. 18) is typically converted to (e.g. Sossi et al., 2019; Ni et al., 2021):

$$ln\frac{C}{C_0} = -\frac{3\alpha_{ec}(1-s)\gamma K}{R_0\rho f(O_2)^{\frac{n}{4}}}\frac{M_{melt}}{\sqrt{M}}\sqrt{\frac{1}{2\pi RT}}t = -kt, \quad (22)$$

with C_0 being the initial concentration of the desired element, and k defined as:

$$k = \frac{3\alpha_{ec}(1-s)\gamma K}{R_0\rho f(O_2)^{\frac{n}{4}}}\frac{M_{melt}}{\sqrt{M}}\sqrt{\frac{1}{2\pi RT}} = \frac{3}{R_0}\nu. \quad (23)$$

Based on eq. (22), the value of k for diffusion-unlimited evaporation experiments can be obtained either by direct calculation using t and $ln\frac{C}{C_0}$, or by plotting $ln\frac{C}{C_0}$ versus time for a time-series of experiments under the same condition. With the value of k being constrained, the value of ν can subsequently be calculated using eq. (23). As a result, the apparent Cu isotope fractionation factors ($\alpha^{63/65}$Cu) and the calculated τ_{Diff}/τ_{Evap} ratios for evaporation experiments from Ni et al. (2021) and Sossi et al. (2020) are plotted in Fig. 5b to be compared with fractionation factor curves at different degrees of vapor saturation (s). Most of the 1300 to 1500 °C experiments in Sossi et al. (2020) fall into the diffusion-unlimited regime with a vapor saturation index between 0.8 and 0.9, except for two experiments conducted under the lowest oxygen fugacity, as being pointed out in the original paper. The apparent Cu isotope fractionation factors of these two experiments, however, appear to be high among all other experiments (Fig. 5b). This contradicts the prediction for the effect of diffusion control and might instead indicate a change in the effective degree of vapor saturation. The evaporation experiments conducted at 2000 °C using a laser levitation apparatus (Ni et al., 2021) had a much higher Cu evaporation rate (k), leading to a higher τ_{Diff}/τ_{Evap} which brings these high temperature experiments to the diffusion-limited regime (Fig. 5b). This could potentially explain the relatively lower $\alpha^{63/65}$Cu values for the laser levitation experiments (Ni et al., 2021) in Fig. 5b, but the role of convection in mass transfer needs to be better quantified to test this possibility (e.g. Ni et al., 2021; Young et al., 2022).

Using a similar approach, the apparent Cu isotope fractionation factor and τ_{Diff}/τ_{Evap} ratio for tektites is also estimated and plotted in Fig. 5b for comparison (see supplementary text for detail). Copper evaporation in tektites is expected to be diffusion-limited due to the larger diameters of tektites (~1 cm) and the high temperature interpreted for their formation (Macris et al., 2018). The fact that the average apparent Cu isotope fractionation factor for tektites lies far above the calculated curve for diffusion-limited evaporation (Fig. 5b) supports convection instead of diffusion as the major form of mass transport during tektite formation. The above conclusion favors volatility as the major factor to explain the varying degrees of depletion for moderately volatile elements in tektites (e.g. Jiang et al., 2019; Ni et al., 2021).

4.4. Implications for diffusion-controlled processes in magmatic systems

In addition to its application to evaporation, Cu isotopic fractionation by diffusion could also be applied to understanding the role of kinetics during Cu-bearing ore deposit formation or fluid-rock interactions. Despite the vast differences in the nature of these processes, they can be simplified to the enrichment and transport of Cu by a second phase in contact with the parental silicate phase that hosts the magmatic Cu. In the case of magmatic sulfide ore deposits, for example, cooling down of a mafic or ultramafic magma in the shallow crust leads to sulfur saturation and the formation of sulfide droplets in the magma. Due to the higher density of the sulfide liquid than the surrounding silicate magma, they sink through the magma chamber and scavenge chalcophile elements, including Cu, from the surrounding magma (Naldrett, 1989). For porphyry-type Cu-bearing ore deposits, a magmatic volatile phase (MVP) forms as the consequence of magma differentiation and decompression, which subsequently rises through the magma chamber due to its low density, simultaneously scavenging ore metals (e.g. Cu, Au, Mo, and Ag) from the parental magma to form ore deposits at shallower depths (Candela, 1997). Literature studies evaluated the potential role of kinetic control on the Cu enrichment processes because the growth and sink of sulfides, or the rise of the MVP in the magma chamber would compete with the diffusive transport of metals from the silicate melt, leading to a potential fractionation of the ore metals as a function of diffusivity (e.g. Mungall, 2002; Huber et al., 2012; Ni and Zhang, 2016; Zhang, 2015; Ni et al., 2017). During alteration of basalts at the seafloor, on the other hand, a seawater-based fluid phase serves at the Cu-scavenging agent, as evidenced by the decreasing Cu concentration from the core to the rim of altered basalt rocks from the southern Mariana and Yap trenches (Guo et al., 2022). Below we demonstrate with a quantitative model how Cu diffusion in silicate melt could

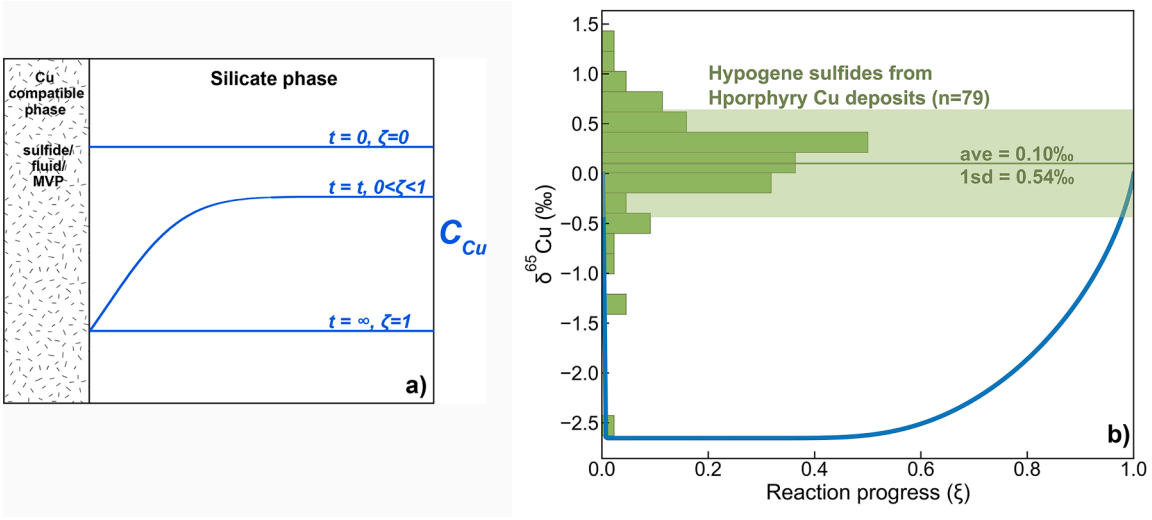

Fig. 6. Illustration of the semi-quantitative model for Cu diffusion and extraction by a second phase in contact with the silicate phase. This second phase would be a sulfide for magmatic sulfide ore deposit formation, a magmatic volatile phase (MVP) for porphyry-type ore deposit formation, or a water-based fluid phase for fluid-basalt interaction. Copper isotope compositions of hypogene sulfides from global porphyry-type ore deposits (Mathur et al., 2005; 2009, 2010, 2012) are plotted in b) for comparison with the model. The δ^{65}Cu data are corrected by the mantle value of 0.07 ‰ (Savage et al., 2015) to obtain fractionation between the ore-forming fluids and the parental mantle.

potentially lead to Cu isotopic fractionation, which can be subsequently utilized to assess the role of kinetics during these magmatic processes.

For the sake of simplicity, we treat the model as linear one-dimensional and we assume the silicate media to have a finite length of L (Fig. 6). Isotopic composition of Cu transported into the Cu-enrichment phase (e.g. sulfide, MVP, or fluid) by diffusion can be solved analytically to be:

$$\delta^{65}\mathrm{Cu} = \left(\frac{1 - \frac{8}{\pi^2}\sum_{n=0}^{\infty} \frac{e^{-(2n+1)^2\pi^2 D_{65} t/L^2}}{(2n+1)^2}}{1 - \frac{8}{\pi^2}\sum_{n=0}^{\infty} \frac{e^{-(2n+1)^2\pi^2 D_{63} t/L^2}}{(2n+1)^2}} - 1 \right) \times 1000‰, \quad (24)$$

where D_{65} and D_{63} are diffusivities of ^{65}Cu and ^{63}Cu, respectively, and the initial δ^{65}Cu of the system is assumed to be 0 ‰. A full derivation of eq. (24) is provided in the supplementary text.

The essential variables in eq. (24) for calculating Cu isotopic composition of the Cu scavenged into the second phase are the diffusivities of ^{65}Cu and ^{63}Cu, the length of the silicate phase (L), and the duration (t). By defining a new parameter of reaction progress ($\zeta = \frac{M_t}{M_\infty} \approx \frac{M_{i,t}}{M_{i,\infty}}$, see supplementary text for definition), however, it is possible to calculate δ^{65}Cu as a function of the reaction progress, which implicitly depends on $D_i t/L^2$. Plotting the calculated δ^{65}Cu versus the reaction progress (ζ) yields a general curve applicable to most situations because the duration can be varied to compensate for different diffusivities or length scales to achieve the same $D_i t/L^2$ for a given value of ζ. The calculated δ^{65}Cu composition of the extracted Cu versus the reaction progress is plotted in Fig. 6b. It can be seen in the figure that the Cu isotopic composition of the lost Cu quickly reaches a steady δ^{65}Cu value of −2.65‰, which is exactly half of the $\Delta_{\mathrm{diffusion}}$ value that is related to the β factor of Cu diffusion in silicate melts via equation:

$$\Delta_{\mathrm{diffusion}} = 1000\left[\left(\frac{m_{63}}{m_{65}}\right)^{\beta} - 1\right] = -5.3‰ \quad (25)$$

The above observation indicates that when the reaction progress is low, diffusion has not reached the other side of the silicate phase and the isotopic fractionation is controlled by a steady diffusion flux at the phase boundary. As the reaction progress increases to 0.5 or higher, however, the system starts to approach equilibrium and the total lost Cu progressively reaches the equilibrium δ^{65}Cu of 0‰ (Fig. 6b). Importantly, due to the high β value for Cu, even at a high reaction progress of 90% equilibrium, the δ^{65}Cu value would still be lower by −1‰ for the Cu-enrichment phase (Fig. 6b). As a result, a diffusion-limited enrichment mechanism for magmatic sulfide or porphyry-type ore deposit formation would lead to a significantly light Cu isotope composition for the ore deposits.

In order to test our model with natural data, Cu isotope data of hypogene sulfides from porphyry-type ore deposits were compiled from the literature and the distribution is plotted in Fig. 6b for comparison. These hypogene sulfides selected for comparison were primary mineral assemblies of chalcocite, pyrite, chalcopyrite, covenite, or bornite formed by the Cu-bearing fluids at relatively high temperatures (Mathur et al., 2012, 2010; 2009, 2005). Most of the 79 hypogene sulfides from porphyry-type ore deposits demonstrate minimal copper isotopic fractionation relative to the mantle δ^{65}Cu composition of 0.07 ‰ (Savage et al., 2015), with an average fractionation of 0.10 ± 0.54 ‰ (2 s.d.), and a median value of 0.14. The low degree of Cu isotopic fractionation between hypogene sulfides and mantle indicates that the parental fluids of porphyry-type ore deposits were dominated by equilibrium enrichment processes.

5. Conclusions

This study reports Cu isotope measurements of diffusion experiments using basaltic glasses. The experimental charges were sampled by a micromill along the diffusion profile and the drilled materials were processed by column chemistry for Cu isotope analysis. Regression of the isotope fractionation profiles using a Monte Carlo approach yield beta factor values of 0.18 ± 0.03 and 0.16 ± 0.03 for the two measured experiments, which are high among all elements studied so far in silicate melts. With a quantitative model for the evaporation of a molten liquid silicate sphere, we show that isotopic fractionation of Cu would be high disregard whether the evaporation is in the diffusion-limited or diffusion-unlimited regime. By combining the model with the Hertz-Knudsen equation, we further show that laboratory evaporation experiments using melt spheres are most likely diffusion-unlimited for Cu, except for those conducted under highly reducing conditions or at high temperatures (e.g. 2000 °C). Tektites are expected to be in the diffusion-limited regime for Cu evaporation, but the high apparent Cu isotope fractionation factors observed for tektites contradict with diffusion being the major form of mass transfer. Instead, convection must have played a dominant role in mass transfer during evaporation of the precursor materials of tektites. We also show quantitatively that magmatic processes involving a second phase enriching Cu from the silicate melt could have a strong Cu isotope fractionation signature if the processes are diffusion-controlled. More specifically, a fractionation of more than −1‰ in δ^{65}Cu is expected even if the degree of equilibrium reaches 90%. Therefore, Cu isotopic compositions can be used as a tool to test for the role of kinetics during magmatic sulfide ore deposit formation, porphyry-type ore deposit formation, or liquid-rock interactions. Compiled Cu isotope data for hypogene sulfides from porphyry-type Cu ore deposits show that their ore-forming fluids appear to be diffusion-unlimited during enrichment and transport to the surface.

CRediT authorship contribution statement

Peng Ni: Writing – review & editing, Writing – original draft, Visualization, Validation, Resources, Methodology, Investigation, Formal analysis, Data curation, Conceptualization. **Anat Shahar:** Writing – review & editing, Supervision, Resources, Methodology, Investigation, Funding acquisition.

Declaration of Competing Interest

The authors declare that they have no known competing financial interests or personal relationships that could have appeared to influence the work reported in this paper.

Data availability

All data used in the paper have been reported in the supplement of the paper

Acknowledgments

P. N. thanks Youxue Zhang, Fang Huang and Heng Chen for early discussions that motivated the work. Mary Horan, Tim Mock, and Michelle Jordan are acknowledged for their assistance in the clean lab and the mass spectrometry lab. We extend sincere thanks to Paolo Sossi for the constructive review and to Raj Dasgupta and Fred Moynier for the editorial handling. P. N. was partially supported by a Carnegie Postdoctoral Fellowship while working on this project. This research is partially supported by NSF EAR grants 1851736 and 2025779 to A. S.

Supplementary materials

Supplementary material associated with this article can be found, in the online version, at doi:10.1016/j.epsl.2023.118459.

References

Candela, P.A., 1997. A review of shallow, ore-related granites: textures, volatiles, and ore Metals. J. Petrol. 1619–1633. https://doi.org/10.1093/petroj/38.12.1619.

Chapman, S., Cowling, T.G., 1970. The Mathematical Theory of Non-Uniform gases; an Account of the Kinetic Theory of viscosity, Thermal Conduction and Diffusion in Gases. Cambridge University Press, 3rd ed. ed.

Crank, J., 1975. The Mathematics of Diffusion, 2nd ed. Oxford University Press.

Dauphas, N., Poitrasson, F., Burkhardt, C., Kobayashi, H., Kurosawa, K., 2015. Planetary and meteoritic Mg/Si and δ30Si variations inherited from solar nebula chemistry. Earth Planet. Sci. Lett. 427, 236–248. https://doi.org/10.1016/j.epsl.2015.07.008.

Day, J.M.D., Moynier, F., Sossi, P.A., Wang, K., Meshik, A.P., Pravdivtseva, O.V., Pettit, D.R., 2020. Moderately volatile element behaviour at high temperature determined from nuclear detonation. Geochem. Perspect. Lett. 13, 54–60.

Day, J.M.D., Sossi, P.A., Shearer, C.K., Moynier, F., 2019. Volatile distributions in and on the Moon revealed by Cu and Fe isotopes in the 'Rusty Rock' 66095. Geochim. Cosmochim. Acta, A GCA special volume in honor of Professor Lawrence A. Taylor 266, 131–143. https://doi.org/10.1016/j.gca.2019.02.036.

Guo, Z., Tian, H.-C., Liu, Y., Peng, X., Qin, G., Lv, Y., 2022. Copper isotopic fractionation during seafloor alteration: insights from altered basalts in the Mariana and Yap trenches. J. Geophys. Res. Solid Earth 127, e2021JB023597. https://doi.org/10.1029/2021JB023597.

Holycross, M.E., Watson, E.B., Richter, F.M., Villeneuve, J., 2018. Diffusive fractionation of Li isotopes in wet, silicic melts. Geochem. Perspect. Lett. 39–42. https://doi.org/10.7185/geochemlet.1807.

Holzheid, A., Lodders, K., 2001. Solubility of copper in silicate melts as function of oxygen and sulfur fugacities, temperature, and silicate composition. Geochim. Cosmochim. Acta 65, 1933–1951. https://doi.org/10.1016/S0016-7037(01)00545-2.

Huber, C., Bachmann, O., Vigneresse, J.-L., Dufek, J., Parmigiani, A., 2012. A physical model for metal extraction and transport in shallow magmatic systems. Geochem. Geophys. Geosystems 13, Q08003. https://doi.org/10.1029/2012GC004042.

Jiang, Y., Chen, H., Fegley, B., Lodders, K., Hsu, W., Jacobsen, S.B., Wang, K., 2019. Implications of K, Cu and Zn isotopes for the formation of tektites. Geochim. Cosmochim. Acta 259, 170–187. https://doi.org/10.1016/j.gca.2019.06.003.

Lodders, K., 2003. Solar system abundances and condensation temperatures of the elements. Astrophys. J. 591, 1220. https://doi.org/10.1086/375492.

Macris, C.A., Asimow, P.D., Badro, J., Eiler, J.M., Zhang, Y., Stolper, E.M., 2018. Seconds after impact: insights into the thermal history of impact ejecta from diffusion between lechatelierite and host glass in tektites and experiments. Geochim. Cosmochim. Acta 241, 69–94. https://doi.org/10.1016/j.gca.2018.08.031.

Marchi, S., Canup, R.M., Walker, R.J., 2018. Heterogeneous delivery of silicate and metal to the Earth by large planetesimals. Nat. Geosci.

Maréchal, C.N., Télouk, P., Albarède, F., 1999. Precise analysis of copper and zinc isotopic compositions by plasma-source mass spectrometry. Chem. Geol. 156, 251–273. https://doi.org/10.1016/S0009-2541(98)00191-0.

Mathur, R., Dendas, M., Titley, S., Phillips, A., 2010. Patterns in the Copper isotope composition of minerals in Porphyry Copper deposits in Southwestern United States. Econ. Geol. 105, 1457–1467. https://doi.org/10.2113/econgeo.105.8.1457.

Mathur, R., Ruiz, J., Casselman, M.J., Megaw, P., van Egmond, R., 2012. Use of Cu isotopes to distinguish primary and secondary Cu mineralization in the Cañariaco Norte porphyry copper deposit. Northern Peru. Miner. Deposita 47, 755–762. https://doi.org/10.1007/s00126-012-0439-y.

Mathur, R., Ruiz, J., Titley, S., Liermann, L., Buss, H., Brantley, S., 2005. Cu isotopic fractionation in the supergene environment with and without bacteria. Geochim. Cosmochim. Acta 69, 5233–5246. https://doi.org/10.1016/j.gca.2005.06.022.

Mathur, R., Titley, S., Barra, F., Brantley, S., Wilson, M., Phillips, A., Munizaga, F., Maksaev, V., Vervoort, J., Hart, G., 2009. Exploration potential of Cu isotope fractionation in porphyry copper deposits. J. Geochem. Explor. 102, 1–6. https://doi.org/10.1016/j.gexplo.2008.09.004.

Moeller, K., Schoenberg, R., Pedersen, R.-B., Weiss, D., Dong, S., 2012. Calibration of the new certified reference materials ERM-AE633 and ERM-AE647 for Copper and IRMM-3702 for Zinc isotope amount ratio determinations. Geostand. Geoanalytical Res. 36, 177–199. https://doi.org/10.1111/j.1751-908X.2011.00153.x.

Moynier, F., Albarède, F., Herzog, G.F., 2006. Isotopic composition of zinc, copper, and iron in lunar samples. Geochim. Cosmochim. Acta, A Special Issue Dedicated to Larry A. Haskin 70, 6103–6117. https://doi.org/10.1016/j.gca.2006.02.030.

Moynier, F., Koeberl, C., Beck, P., Jourdan, F., Telouk, P., 2010. Isotopic fractionation of Cu in tektites. Geochim. Cosmochim. Acta 74, 799–807. https://doi.org/10.1016/j.gca.2009.10.012.

Moynier, F., Vance, D., Fujii, T., Savage, P., 2017. The Isotope geochemistry of Zinc and Copper. Rev. Mineral. Geochem. 82, 543–600. https://doi.org/10.2138/rmg.2017.82.13.

Mungall, J.E., 2002. Kinetic controls on the partitioning of trace elements between Silicate and Sulfide liquids. J. Petrol. 43, 749–768. https://doi.org/10.1093/petrology/43.5.749.

Naldrett, A.J., 1989. Magmatic Sulfide Deposits. Oxford University Press, U.K.

Ni, H., Shi, H., Zhang, L., Li, W.-C., Guo, X., Liang, T., 2018. Cu diffusivity in granitic melts with application to the formation of porphyry Cu deposits. Contrib. Mineral. Petrol. 173, 50. https://doi.org/10.1007/s00410-018-1475-0.

Ni, P., Macris, C.A., Darling, E.A., Shahar, A., 2021. Evaporation-induced copper isotope fractionation: insights from laser levitation experiments. Geochim. Cosmochim. Acta 298, 131–148. https://doi.org/10.1016/j.gca.2021.02.007.

Ni, P., Zhang, Y., 2016. Cu diffusion in a basaltic melt. Am. Mineral. 101, 1474–1482. https://doi.org/10.2138/am-2016-5544.

Ni, P., Zhang, Y., Simon, A., Gagnon, J., 2017. Cu and Fe diffusion in rhyolitic melts during chalcocite "dissolution": implications for porphyry ore deposits and tektites. Am. Mineral. 102, 1287–1301. https://doi.org/10.2138/am-2017-5885.

Nie, N.X., Dauphas, N., 2019. Vapor drainage in the protolunar disk as the cause for the depletion in volatile elements of the moon. Astrophys. J. 884, L48. https://doi.org/10.3847/2041-8213/ab4a16.

Norris, C.A., Wood, B.J., 2017. Earth's volatile contents established by melting and vaporization. Nature 549, 507–510. https://doi.org/10.1038/nature23645.

Richter, F.M., Dauphas, N., Teng, F.-Z., 2009. Non-traditional fractionation of non-traditional isotopes: evaporation, chemical diffusion and Soret diffusion. Chem. Geol 258, 92–103. https://doi.org/10.1016/j.chemgeo.2008.06.011. Applications of non-traditional stable isotopes in high-temperature geochemistry.

Richter, F.M., Davis, A.M., DePaolo, D.J., Watson, E.B., 2003. Isotope fractionation by chemical diffusion between molten basalt and rhyolite. Geochim. Cosmochim. Acta 67, 3905–3923. https://doi.org/10.1016/S0016-7037(03)00174-1.

Richter, F.M., Liang, Y., Davis, A.M., 1999. Isotope fractionation by diffusion in molten oxides. Geochim. Cosmochim. Acta 63, 2853–2861. https://doi.org/10.1016/S0016-7037(99)00164-7.

Richter, F.M., Watson, E.B., Mendybaev, R.A., Teng, F.-Z., Janney, P.E., 2008. Magnesium isotope fractionation in silicate melts by chemical and thermal diffusion. Geochim. Cosmochim. Acta 72, 206–220. https://doi.org/10.1016/j.gca.2007.10.016.

Rodovská, Z., Magna, T., Žák, K., Kato, C., Savage, P.S., Moynier, F., Skála, R., Ježek, J., 2017. Implications for behavior of volatile elements during impacts—Zinc and copper systematics in sediments from the Ries impact structure and central European tektites. Meteorit. Planet. Sci. 52, 2178–2192. https://doi.org/10.1111/maps.12922.

Savage, P.S., Moynier, F., Chen, H., Shofner, G., Siebert, J., Badro, J., Puchtel, I.S., 2015. Copper isotope evidence for large-scale sulphide fractionation during Earth's differentiation. Geochem. Perspect. Lett. 10.7185/geochemlet.1506.

Siebert, J., Corgne, A., Ryerson, F.J., 2011. Systematics of metal–silicate partitioning for many siderophile elements applied to Earth's core formation. Geochim. Cosmochim. Acta 75, 1451–1489. https://doi.org/10.1016/j.gca.2010.12.013.

Sossi, P.A., Halverson, G.P., Nebel, O., Eggins, S.M., 2015. Combined separation of Cu, Fe and Zn from rock matrices and improved analytical protocols for stable isotope determination. Geostand. Geoanalytical Res. 39, 129–149. https://doi.org/10.1111/j.1751-908X.2014.00298.x.

Sossi, P.A., Klemme, S., O'Neill, H.St.C., Berndt, J., Moynier, F., 2019. Evaporation of moderately volatile elements from silicate melts: experiments and theory. Geochim. Cosmochim. Acta 260, 204–231. https://doi.org/10.1016/j.gca.2019.06.021.

Sossi, P.A., Moynier, F., Treilles, R., Mokhtari, M., Wang, X., Siebert, J., 2020. An experimentally-determined general formalism for evaporation and isotope fractionation of Cu and Zn from silicate melts between 1300 and 1500 °C and 1 bar. Geochim. Cosmochim. Acta 288, 316–340. https://doi.org/10.1016/j.gca.2020.08.011.

Teng, F.-Z., Dauphas, N., Watkins, J.M., 2017. Non-traditional stable isotopes: retrospective and prospective. Rev. Mineral. Geochem. 82, 1–26. https://doi.org/10.2138/rmg.2017.82.1.

Watkins, J.M., DePaolo, D.J., Huber, C., Ryerson, F.J., 2009. Liquid composition-dependence of calcium isotope fractionation during diffusion in molten silicates. Geochim. Cosmochim. Acta 73, 7341–7359. https://doi.org/10.1016/j.gca.2009.09.004.

Watkins, J.M., DePaolo, D.J., Ryerson, F.J., Peterson, B.T., 2011. Influence of liquid structure on diffusive isotope separation in molten silicates and aqueous solutions. Geochim. Cosmochim. Acta 75, 3103–3118. https://doi.org/10.1016/j.gca.2011.03.002.

Watkins, J.M., DePaolo, D.J., Watson, E.B., 2017. Kinetic fractionation of non-traditional stable isotopes by diffusion and crystal growth reactions. Rev. Mineral. Geochem. 82, 85–125. https://doi.org/10.2138/rmg.2017.82.4.

Young, E.D., Macris, C.A., Tang, H., Hogan, A.A., Shollenberger, Q.R., 2022. Isotope velocimetry: experimental and theoretical demonstration of the potential importance of gas flow for isotope fractionation during evaporation of protoplanetary material. Earth Planet. Sci. Lett. 589, 117575 https://doi.org/10.1016/j.epsl.2022.117575.

Young, E.D., Nagahara, H., Mysen, B.O., Audet, D.M., 1998. Non-Rayleigh oxygen isotope fractionation by mineral evaporation: theory and experiments in the system SiO2. Geochim. Cosmochim. Acta 62, 3109–3116. https://doi.org/10.1016/S0016-7037(98)00213-0.

Young, E.D., Shahar, A., Nimmo, F., Schlichting, H.E., Schauble, E.A., Tang, H., Labidi, J., 2019. Near-equilibrium isotope fractionation during planetesimal evaporation.

Zajacz, Z., Seo, J.H., Candela, P.A., Piccoli, P.M., Tossell, J.A., 2011. The solubility of copper in high-temperature magmatic vapors: a quest for the significance of various chloride and sulfide complexes. Geochim. Cosmochim. Acta 75, 2811–2827. https://doi.org/10.1016/j.gca.2011.02.029.

Zhang, Y., 2022. Diffusive fractionation of K isotopes in molten basalts. Earth Planet Sci. Lett. 581, 117405 https://doi.org/10.1016/j.epsl.2022.117405.

Zhang, Y., 2015. Toward a quantitative model for the formation of gravitational magmatic sulfide deposits. Chem. Geol. 391, 56–73. https://doi.org/10.1016/j.chemgeo.2014.10.025.

Zhang, Y., Ni, H., Chen, Y., 2010. Diffusion data in Silicate melts. Rev. Mineral. Geochem. 72, 311–408. https://doi.org/10.2138/rmg.2010.72.8.

Zhang, Z.J., Nie, N.X., Mendybaev, R.A., Liu, M.-C., Hu, J.J., Hopp, T., Alp, E.E., Lavina, B., Bullock, E.S., McKeegan, K.D., Dauphas, N., 2021. Loss and isotopic fractionation of alkali elements during diffusion-limited evaporation from molten silicate: theory and experiments. ACS Earth Space Chem 5, 755–784. https://doi.org/10.1021/acsearthspacechem.0c00263.